Title
Crack healing in cross-ply composites observed by dynamic mechanical analysis

Authors
Nielsen, C
Nemat-Nasser, S

Publication Date
2015

DOI
10.1016/j.jmps.2014.11.006

Peer reviewed

Crack healing in cross-ply composites observed by dynamic mechanical analysis

Christian Nielsen* and Sia Nemat-Nasser

Department of Mechanical and Aerospace Engineering, University of California at San Diego, 9500 Gilman Drive, La Jolla, CA 92093-0416, USA

Phone: (858) 534-5918

Fax: (858) 534-2727

Email: cenielsen@ucsd.edu*, sia@ucsd.edu

Cross-ply composites with healable polymer matrices are characterized using dynamic mechanical analysis (DMA). The $[90,0]_s$ samples are prepared by embedding layers of unidirectional glass or carbon fibers in 2MEP4FS, a polymer with thermally reversible covalent cross-links previously shown to be capable of healing internal cracks and fully recovering fracture toughness under ideal conditions. After fabrication, cracks in the composites' transverse plies are observed and attributed to residual thermal stresses introduced during processing. Single cantilever bending DMA measurements show the samples exhibit periods of increasing storage moduli with increasing temperature. These results are accurately modeling using simple one-dimensional composite and beam analyses. The effect of cracks on the measured stiffness is considered using a shear lag model, and the predicted crack density of the glass fiber composite falls within a range estimated by microscopy observations. Crack healing is assumed to occur as a function of temperature, and rationales for the onset and conclusion of healing are given.

Keywords: Diels-Alder reaction, fiber-reinforced composite material, beams and columns, microcracking, mechanical testing

1. Introduction

Fiber-reinforced composite materials are popular in structural applications due to their strength and light weight. They are composed of strengthening fibers embedded in a matrix material that facilitates load sharing. Due to mechanical and thermal property mismatches, composite materials are notoriously susceptible to microcrack damage. Through cyclic loading, these microcracks will grow, coalesce into larger cracks, and ultimately lead to structural failure. Current technology relies on identifying cracks and manual repair or replacement of the composite. If the microcracks could instead be healed before they grow, the useful life of the composite could be extended. This would be particularly useful in foreign environments where human intervention is difficult or impossible.

There are currently two general approaches to creating a composite material that is self-healing or healable via external stimuli. The first approach is to embed liquid healing agent that can bleed out into a crack or other damage and mitigate it. White et al. (2001) incorporated catalyst particles and microcapsules containing a healing agent into a polymer material which could serve as the matrix in a fibrous composite. Pang and Bond (2005) moved the healing agent out of the matrix and into hollow fibers. In these two approaches, once the healing agent bleeds out into the damaged region and hardens, there is no more available if new damage subsequently forms in the same location. To overcome this limitation, Toohey et al. (2007) investigated using embedded microvascular networks where healing agent can be pumped to the damage site in a biomimetic process. The second approach to creating a healable composite material is through the use of a polymer matrix which can re-form broken cross-linking bonds. This is a fundamentally different process than the flowing of polymer chains to heal damage in a thermoplastic material (Wool and O'Conner, 1981). Plaisted and Nemat-Nasser (2007) have

demonstrated full recovery of fracture resistance after healing cracks in a neat polymer that uses thermally reversible Diels-Alder (DA) adducts as cross-linking bonds. Plaisted studied 2MEP4FS, a polymer formed from two monomers reacting in a Diels-Alder cycloaddition (Chen et al., 2002; Chen et al., 2003). Since healing was performed at temperatures below where the DA adducts separate, the process requires the crack faces to remain matched and abutted. As the matrix material in a composite, the fibers could help hold the crack surfaces together. These conditions should facilitate healing.

Plaisted (2007) also demonstrated crack healing in 2MEP4FS reinforced with glass and carbon fibers. The composite samples were characterized using single cantilever bending dynamic mechanical analysis. After subsequently subjecting them to cold temperature treatments to introduce microcracks, the samples were recharacterized. They were healed using an elevated temperature thermal treatment and characterized a third time. The composite samples were found to recover a significant portion of the originally measured stiffness. Park et al. (2009) used a single component, DA-based polymer as the matrix in a carbon fiber composite. The sample was subjected to 3-point bending to measure the stiffness and create cracks. The cracks were healed by using the carbon fiber as an embedded resistive heater. The process was repeated several times and most of the original stiffness was recovered each time.

In studying composite healing, both Plaisted and Park focused on observing changes in mechanical properties after cracking and healing. They did not correlate the number of cracks with the measured mechanical properties. Particularly in Plaisted's study where numerous cracks were present, correlation of the cracks with the measured flexural storage modulus would have been useful in estimating how many cracks were formed and healed by the thermal treatments. A number of analysis techniques have been developed for estimating the mechanical

degradation caused by cracks in cross-ply composites like those considered by Plaisted. Broadly termed "finite fracture mechanics" (Hashin, 1996), these techniques use each crack as the incremental unit of damage rather than differential crack extension as in classical fracture mechanics. Every new crack is assumed to extend through the ply thickness and be arrested by the boundary conditions without causing failure of the composite. In one-dimensional shear lag methods, the load is transferred from a longitudinal ply to a cracked transverse ply by shear stresses which are a function of distance from the crack (Highsmith and Reifsnider, 1982; Laws and Dvorak, 1988). Two-dimensional variational methods for stress analysis have also been developed (Hashin, 1986; Nairn and Hu, 1992).

In the present work, carbon and glass fiber composites with 2MEP4FS matrices are prepared, characterized, and the mechanical results are compared with simple one-dimensional analyses. It's found that not only cracks, but also crack healing must be considered to fully explain the experimentally observed behavior.

2. Experimentation

2.1. Sample preparation

Composite samples were prepared using a prepreg process to create and laminate multiple layers of unidirectional fiber and 2MEP4FS polymer matrix. Each sample was formed from prepreg layers containing either Toray T300 carbon fiber or AGY S-2 glass fiber. The properties of each composite constituent are given in Table 1.

The prepreg process was developed as an extension of the small-sample 2MEP4FS processing method outlined by Nielsen et al. (2014). This method allows small quantities of polymer to be produced with precise monomer ratios and minimal wasted material. The bismaleimide and tetrafuran monomers had been previously synthesized according to standard

Table 1. Composite constituent properties.

	Carbon Fiber[a,b] $x = f$	Glass Fiber[c] $x = f$	2MEP4FS[d,e] $x = m$
Mass density, ρ_x	1.76 g/cm^3	2.488 g/cm^3	1.347 g/cm^3
Longitudinal Young's modulus, E_{xL}	230 GPa	93.8 GPa	3.046 GPa
Transverse Young's modulus, E_{xT}	22 GPa	93.8 GPa	3.046 GPa
Poisson's ratio, ν_x	0.35	0.23	0.367
Shear modulus, G_x	22 GPa	38.1 GPa	1.114 GPa
Longitudinal CTE, α_{xL}	-1.3 μm/m/°C	1.6 μm/m/°C	41 μm/m/°C
Transverse CTE, α_{xT}	7.0 μm/m/°C	1.6 μm/m/°C	41 μm/m/°C

a. Kaw, 2006
b. Toray Carbon Fibers America Inc, 2012
c. AGY, 2006
d. Plaisted, 2007
e. Nielsen, 2012

procedures (Chen et al., 2002; Weizman et al., 2011). For each composite sample, two prepolymer batches were prepared in parallel to increase the quantity of prepolymer. Approximately 600 mg were produced for each composite. A small stoichiometric quantity of monomers were mixed in two glass culture tubes and subjected to high vacuum. The tubes were lowered into a 90 °C oil bath, where the bismaleimide melted and further mixed with the tetrafuran as the polymerization began. The homogenous prepolymers were quenched in liquid nitrogen and returned to room temperature, where they were transferred to a nylon film bag containing a layer of unidirectional fiber. High vacuum was applied to the bag, bringing together the fibers and prepolymer. Still under vacuum, the bag was briefly placed on a steel surface preheated to 90 °C, and the prepolymer was forced into the fibers using a brayer. The bag and thin sample were quickly cooled to room temperature and prepreg layers were cut out in the desired orientations.

The prepreg layers were immediately stacked in a $[90,0]_s$ cross-ply sequence. Since intralaminar cracks tend to form parallel with the fiber orientation, the outer 90° plies served to

amplify the effect of cracks on bending measurements where the maximum tensile and compressive stresses are at the outer surfaces. The inner 0° plies allowed the samples to retain structural integrity after the formation of cracks in each ply. The stacked layers were placed beneath an aluminum piston in a 0.5 by 1.5 inch opening in an aluminum mold. The mold and piston had been lightly seasoned with Slide Universal Mold Release. Differential scanning calorimetry (DSC) studies show no effect of the mold release treatment on the thermal properties of cured 2MEP4FS, indicating no solvents or other plasticizers were being introduced. The assembled aluminum mold was placed in a preheated press, and a minimum pressure to ensure good contact was applied to the piston. A thermocouple placed in the mold near the sample indicated that the sample temperature varied from 90 to 95 °C during the curing process. The pressure was also monitored, and regularly adjusted as necessary to keep it low, while maintaining the contact of the mold with the upper and lower steel platens. After three hours, the press was turned off and the mold and sample were allowed to slowly cool to room temperature over a period of approximately 6 hours. The sample was removed from the mold, cured for an additional 2 hours in a preheated 90 °C oven, and slowly cooled to room temperature again over approximately 10 hours.

The cured composite samples were mounted in a Struers Automated Polishing System and the edges were ground down approximately 0.6 mm to reach the transverse fibers and then polished with successively finer grit sandpapers. Final polishing was performed using a 1 μm alumina slurry. After polishing, the samples were washed with purified water and dried.

2.2. Characterization

The physical, thermal, and mechanical properties of the polished composite samples were measured. The dimensions of each sample were recorded, and the densities determined using the

sample masses and volumes of water displaced by the samples. Assuming no voids, the overall fiber volume fraction, V_f, was estimated using the measured sample density, ρ_s, the known densities of the constituent materials (ρ_f, ρ_m), and the rule of mixtures:

$$V_f = \frac{\rho_s - \rho_m}{\rho_f - \rho_m}. \quad (1)$$

The carbon fiber and glass fiber composites had similar overall fiber volume fractions: 0.571 and 0.576 respectively.

2.2.1. Microscopy

The composite samples were inspected and photographed using a Nikon Epiphot inverted metallograph. Very few voids were observed, and they were mostly near the outer unpolished surfaces. Cracks were observed in both samples before any mechanical experiments were performed (Figure 1). The cracks were mostly closed, appearing as fine lines in the images. Only a few were found by inspecting microscopy images. The semi-transparent glass fiber sample was also imaged through-thickness with a high resolution scanner (Figure 2). Striations in the longitudinal and transverse directions indicate the presence of numerous cracks. The carbon fiber sample was opaque, so a similar through-thickness characterization was not possible.

The average transverse and longitudinal ply thicknesses were estimated from metallograph images. In both samples, the longitudinal plies were observed to be thinner than the transverse plies. Since the longitudinal and transverse prepreg layers were prepared together, they are assumed to have similar initial thicknesses. The discrepancy may be the result of the prepolymer more easily flowing along the fiber direction when pressure was applied, or the prepolymer being drawn to the hot aluminum mold surfaces at the top and bottom of the sample during the initial, low viscosity stage of curing. Since the fiber quantity in each ply should be constant

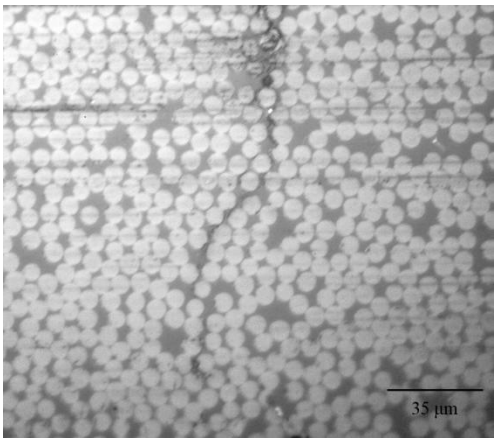

Fig. 1. Optical microscope image of a transverse ply crack in the carbon fiber composite sample. The crack runs from the top center to the bottom of the image.

Fig. 2. Through-thickness view of the glass fiber composite sample. The longitudinal plies are oriented left-right in the image.

given the unidirectional fiber tape used, the thickness of the layers must be considered in determining the fiber volume fraction of each layer. The estimates made using mass density can be separated into longitudinal fiber volume fraction:

$$V_{Lf} = V_f \frac{2(t_L+t_T)}{4t_L}, \tag{2a}$$

and transverse fiber volume fraction:

$$V_{Tf} = V_f \frac{2(t_L+t_T)}{4t_T}, \tag{2b}$$

where t_L and t_T are the average thicknesses of the longitudinal and transverse plies. The updated fiber volume fraction estimates are given in Table 2. Fiber volume fractions in the transverse

plies were also estimated from photographs. The results are reasonably close to the fiber volume fraction estimates derived from the density method, varying by a few percent. These measurements were made from only a few photographs, and voids were not considered.

2.2.2. Differential scanning calorimetry

Thermal measurements were made using a TA Instruments 2920 Differential Scanning Calorimeter (DSC) configured with a liquid nitrogen cooling accessory and 50 mL/min dry nitrogen purge gas. A corner of each composite sample was cut off, individually sealed in a hermetic aluminum pan, and heated at 3 °C/min with ±1 °C/min sinusoidal modulation from 0 °C through the glass transition temperature, T_g, taken here as the inflection of the reversible part of the measured heat flow (TA Instruments, 1998). The glass transition temperatures of the carbon fiber and glass fiber composites were 94.7 °C and 100.8 °C respectively. Applying the previously determined model for 2MEP4FS cross-linking as a function of T_g (Nielsen et al., 2014) gives conversions of 0.956 and 0.998, where 1 indicates a fully cured sample. The relatively low final conversion of the carbon fiber composite may be due to the increased surface area of the smaller diameter carbon fibers and more sizing transferring into the polymer and acting as a plasticizer. Nearly ideal results for the glass fiber composite indicate that the sparse fill threads holding the fibers together did not affect the final polymer matrix. Plaisted (2007) also noted inconsistent DSC thermal results from his carbon fiber composite. Here, the change is deemed small and ignored for the purposes of analysis.

2.2.3. Dynamic mechanical analysis

Mechanical measurements were made using a TA Instruments 2980 Dynamic Mechanical Analyzer (DMA). The composite samples were tested in the single cantilever bending configuration, where both ends are fixed against rotation and one end of the sample is moved up

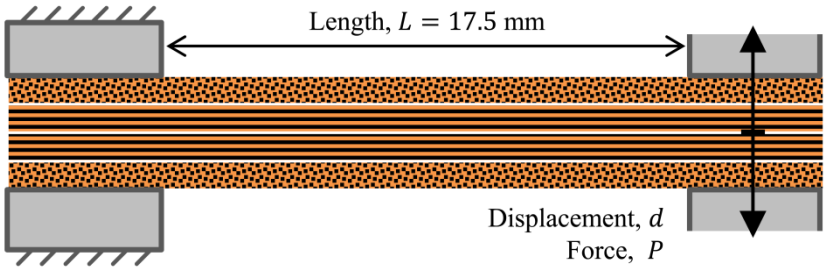

Fig. 3. Diagram of single cantilever bending DMA measurements made on the composite samples.

and down (Figure 3). Each sample was mounted in the rear position of the dual cantilever bending clamp, and the clamp screws were tightened with 8 in·lbf of torque. The instrument's thermocouples were positioned near the sample for temperature measurements. A multi-frequency scan of 0.1, 1, 2, 5, 10, and 20 Hz was performed with a displacement amplitude of ±10 μm. In this mode of operation, the instrument uses the prescribed displacement amplitude and the measured force and time lag between signals to determine the storage modulus, E', and loss modulus, E'', of the sample. The DMA calculates the storage modulus of the sample using one-dimensional Euler-Bernoulli beam theory with additional non-dimensional terms to account for imperfect fixation at the grips and shear deformation (TA Instruments, 2002):

$$E' = \frac{PL^3}{12Id}\frac{1}{F_c}\left[1 + \frac{12}{5}(1+\nu)\left(\frac{t}{L}\right)^2\right] \tag{3}$$

where d is the prescribed displacement, P is the measured force, I is the second moment of area, and F_c is a clamping correction factor.

The scan was performed eight times, with the sample removed and remounted in a different orientation each time. The measurements were made at room temperature with the furnace open. This method was verified using a single cantilever polycarbonate standard sample provided by TA Instruments. The results of a single frequency measurement at room temperature with the

furnace open match the reference data provided by TA Instruments. The average storage and loss moduli for the 2MEP4FS composite samples are given in Figure 4.

After multi-frequency testing, the samples were remounted a final time in the DMA and scanned with the furnace closed at 1 Hz from 20 °C to 130 °C at 3 °C/min. The resulting storage moduli and $\tan\delta$ are given in Figure 5. Both samples show an initial decrease, then increase, peak, and strong decrease in storage moduli as the temperature increases. This behavior was unexpected as the 2MEP4FS matrix only exhibits a decreasing storage modulus with temperature when tested alone (Nielsen, 2012). The mechanical properties of the fibers were not expected to

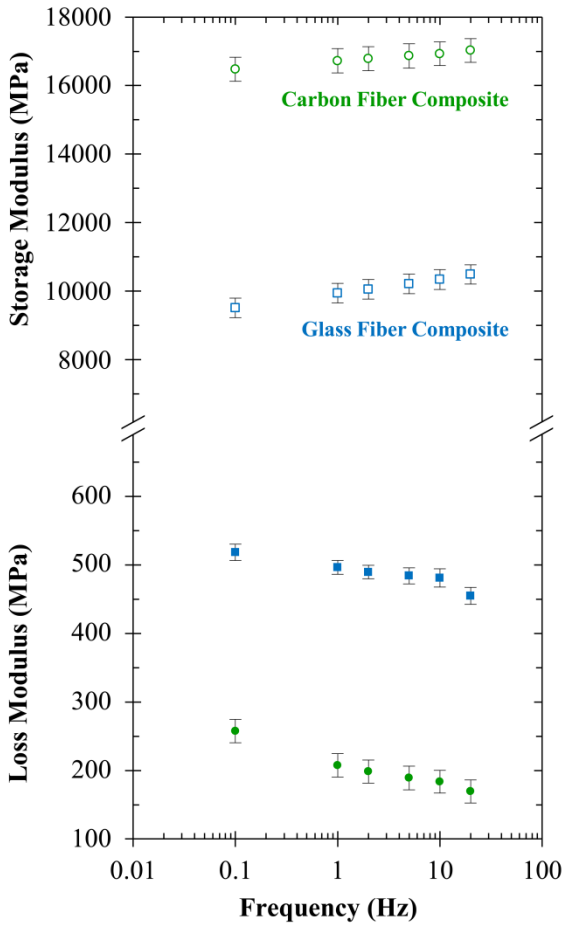

Fig. 4. Room temperature DMA results for the carbon and glass fiber composites as a function of frequency.

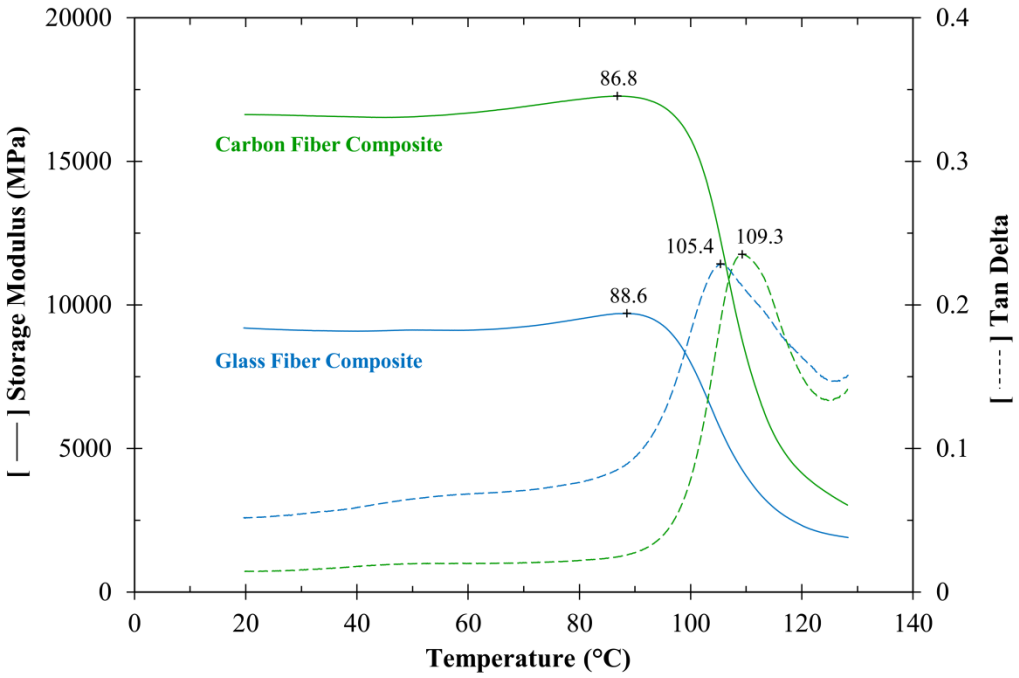

Fig. 5. Single frequency (1 Hz) DMA results for the carbon and glass fiber composites as a function of temperature.

vary significantly over this temperature range. These results are explored and explained in the following analyses.

3. Analysis

The composites are analyzed using simple one-dimensional approximations for comparison with the one-dimensional DMA experimental results. Below the glass transition temperature, T_g, the loss moduli of the samples were observed to be small compared with the storage moduli; i.e. $\tan\delta$ was small. Therefore, the samples are treated as linear elastic, and the storage modulus is taken as Young's modulus for the purpose of calculations. The fibers and matrix are homogenized to form a single material with effective properties for the transverse and longitudinal directions of each ply. The samples are first treated as fully intact, the ideal case.

The effect of transverse cracks is subsequently considered using a shear lag model, and the effective tensile moduli of the damaged transverse plies are estimated as a function of crack density. Crack healing is finally included as a linear function of temperature. The effective properties of the transverse and longitudinal plies are homogenized to form a single beam with effective properties. This beam is considered as an Euler-Bernoulli beam in bending with small displacements. The results of the homogenization estimates and DMA measurements are compared.

3.1. Ideal, intact composite

As a first approximation, the composite samples are treated as fully intact with no cracks affecting the mechanical properties. Using the constituent properties (Table 1), fiber volume fractions, and sample dimensions, the fibers and matrix of each ply are homogenized using standard strength of materials methods to obtain effective properties (Kaw, 2006). The sample geometry and a representative volume element are depicted in Figure 6. In the following notation, the first subscript refers to the ply (T, L) or constituent (f, m) and the second subscript

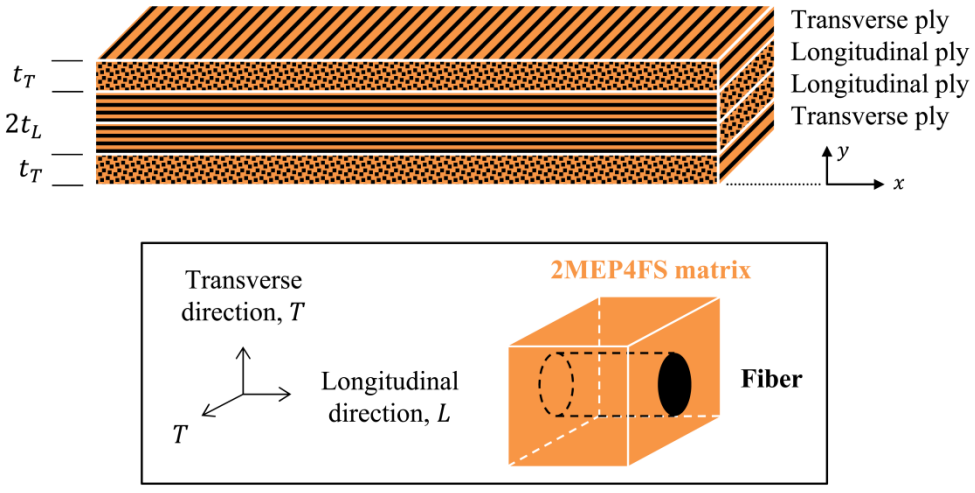

Fig. 6. The layup of each composite and a representative volume element of the fiber and matrix.

denotes the direction (T, L) or constituent (f, m).

The effective Young's modulus in the longitudinal direction of each ply is determined using the Voigt model, where the strain of each constituent is assumed constant and the overall stiffness is given by the rule of mixtures:

$$E_{LL} = V_{Lf}E_{fL} + \left(1 - V_{Lf}\right)E_{mL}, \tag{4a}$$

$$E_{TL} = V_{Tf}E_{fL} + \left(1 - V_{Tf}\right)E_{mL}. \tag{4b}$$

Conversely, the effective Young's modulus in the transverse direction of each ply is determined using the Reuss model, where the stress in each constituent is assumed constant and the overall compliance is given by the rule of mixtures:

$$\frac{1}{E_{LT}} = \frac{V_{Lf}}{E_{fT}} + \frac{1-V_{Lf}}{E_{mT}}, \tag{5a}$$

$$\frac{1}{E_{TT}} = \frac{V_{Tf}}{E_{fT}} + \frac{1-V_{Tf}}{E_{mT}}. \tag{5b}$$

The effective Poisson's ratio and shear modulus of the longitudinal plies in the plane of bending are determined using the rule of mixtures:

$$\nu_{LT} = V_{Lf}\nu_f + \left(1 - V_{Lf}\right)\nu_m, \tag{6}$$

$$G_{LT} = \left(\frac{V_{Lf}}{G_f} + \frac{1-V_{Lf}}{G_m}\right)^{-1}. \tag{7}$$

The effective Poisson's ratio and shear modulus for the transverse plies in the plane of bending (ν_{TT}, G_{TT}) were also estimated using the rule of mixtures and a simple isotropic assumption. Given the fiber-matrix geometry of the transverse direction of the transverse plies, these assumptions for ν_{TT} and G_{TT} are generally not appropriate estimates of effective properties. Micromechanics methods given by Nemat-Nasser and Hori (1999) are better approximations. The self-consistent method for a random distribution of aligned reinforcing microfibers includes interaction between the fibers. Using this method, the effective transverse ply Poisson's ratio,

ν_{TT}, can be extracted from the overall bulk modulus, and the effective shear modulus, G_{TT}, can be determined. The micromechanics method estimates the transverse shear moduli of both samples to be on the order of 2 GPa, which is comparable to the estimate made here. The shear modulus controls the number of estimated cracks in later calculations. The calculated mechanical properties for each composite are given in Table 2.

The homogenized layers are considered as plies in a rectangular $[90,0]_s$ composite beam subjected to bending (Figure 3). The samples are thin and the experimental displacements were small relative to the sample length, so one-dimensional Euler-Bernoulli beam theory applies. The neutral axis, $\bar{y}$, of the beam is located where the axial force due to bending is zero:

$$\int_T \sigma_{TL}(y)dA + \int_L \sigma_{LL}(y)dA = 0, \tag{8}$$

Table 2. Homogenized lamina properties.

		Carbon Fiber Composite	Glass Fiber Composite
Longitudinal Ply	Thickness, t_L	0.165 mm	0.153 mm
	Fiber volume fraction, V_{Lf}	0.623	0.623
	Longitudinal Young's modulus, E_{LL}	144 GPa	59.6 GPa
	Transverse Young's modulus, E_{LT}	6.58 GPa	7.67 GPa
	LT-plane Poisson's ratio, ν_{LT}	0.325	0.282
	LT-plane shear modulus, G_{LT}	2.73 GPa	2.82 GPa
	Longitudinal CTE, α_{LL}	-0.96 μm/m/°C	2.36 μm/m/°C
	Transverse CTE, α_{LT}	41.1 μm/m/°C	35.3 μm/m/°C
Transverse Ply	Thickness, t_T	0.196 mm	0.178 mm
	Fiber volume fraction, V_{Tf}	0.527	0.536
	Longitudinal Young's modulus, E_{TL}	123 GPa	51.6 GPa
	Transverse Young's modulus, E_{TT}	5.58 GPa	6.32 GPa
	TT-plane Poisson's ratio, ν_{TT}	0.358	0.294
	TT-plane shear modulus, G_{TT}	2.05 GPa	2.44 GPa
	Longitudinal CTE, α_{TL}	-0.68 μm/m/°C	2.32 μm/m/°C
	Transverse CTE, α_{TT}	34.7 μm/m/°C	30.3 μm/m/°C

where A is the cross-sectional area of the beam. Since the ideal, intact beam is symmetric both in geometry and material properties, the neutral axis will be at the center of the beam:

$$\bar{y} = t_L + t_T. \tag{9}$$

The moment-curvature relationship is:

$$E_{flex} I\kappa = \int_T \sigma_{TL}(y) y dA + \int_L \sigma_{LL}(y) y dA, \tag{10}$$

where κ is the curvature, which is approximated as constant through the thickness of the beam. The overall flexural modulus of the intact beam is found to be:

$$E_{flex} = \frac{8E_{TT}t_T\left(3t_L^2+3t_L t_T+t_T^2\right)+8E_{LL}t_L^3}{(t_L+t_T)^3}. \tag{11}$$

The Euler-Bernoulli flexural moduli were compared with estimates given by laminated plate theory and found to be in very good agreement (< 0.5 % difference).

The calculated flexural moduli are compared with the DMA storage moduli measured at 1 Hz at room temperature. Although the calculations are for static cases, the 2MEP4FS moduli were determined using DMA at 1 Hz. Assuming the carbon and glass fiber moduli are independent of frequency, the comparison is appropriate. The carbon fiber composite sample is predicted to have a modulus 14 % higher than measured, and the glass fiber composite sample is predicted to have a modulus 26 % higher than measured. In the literature, it has been noted that unidirectional fiber that has been sitting out at atmospheric conditions for extended periods of time will yield composites with poor bonding between the fibers and matrix, likely due to moisture accumulation at the fiber surface (Sjögren and Berglund, 2000). To rule out interfacial problems, new unidirectional S-2 glass fiber tape was purchased and stored under high vacuum. This fiber was used to produce a third composite sample, which was prepared and characterized in a similar manner. The DMA single cantilever bending results show a comparable reduction in

stiffness relative to the calculated properties, suggesting moisture at the interface is not a concern.

The calculated flexural moduli and measured DMA storage moduli for the composite samples are also compared as a function of temperature. The storage modulus of neat 2MEP4FS was previously characterized at 1 Hz as a function of temperature, from 20 °C to 130 °C at 3 °C/min (Nielsen, 2012). These experimental parameters are the same for the composite DMA measurements. Assuming changes in fiber properties as a function of temperature were minimal, the ply and beam properties, equations (4a), (5b), and (11), are evaluated as a function of temperature. Comparing the calculated and measured moduli, the values are initially in poor agreement, but converge between 90 °C and 100 °C (Figure 12). Beyond the glass transition temperature, the calculations and experiments can no longer be meaningfully compared. At the T_g of 2MEP4FS, the storage modulus precipitously drops and $\tan\delta$ sharply increases, precluding further consideration of the polymer as a linear elastic material. Softening of the polymer and composite samples also leads to viscous deformation in the compressed gripped regions. Since the experiment is sensitive to sample thickness, this deformation quickly skews the measured flexural moduli.

3.2. Composite with cracks

The discrepancy between the calculated flexural moduli for the ideal, intact case and the measured storage moduli at room temperature may be attributed to the presence of cracks in the composite plies. Cracks were seen in microscopy images of the transverse plies in both the glass fiber and carbon fiber composite samples. The transverse plies are the furthest from the neutral axis and the cracks are oriented along the fiber direction, normal to the plane of bending, meaning the observed damage would have a significant effect on the DMA measurements.

Since the cracks were observed before any mechanical measurements had been performed, the damage must have occurred during sample preparation. The samples were gently removed from the aluminum mold and tightly clamped with only the edges exposed during polishing, so crack formation during these steps is unlikely. The samples had been cured at a maximum temperature of 95 °C and then cooled to room temperature for characterization. Residual thermal stresses due to differences in the coefficient of thermal expansion (CTE), α, between the constituents and between the cross-oriented plies could be the source of the observed cracks. Specifically, the CTE of 2MEP4FS is an order of magnitude higher than both the carbon and glass fibers (Table 1). An effective CTE for each ply is determined following similar strength of materials homogenization methods as previously employed (Kaw, 2006). The longitudinal CTE for each ply is:

$$\alpha_{LL} = V_{Lf}\left(\frac{\alpha_{fL}E_{fL}}{E_{LL}}\right) + \left(1 - V_{Lf}\right)\left(\frac{\alpha_{mL}E_{mL}}{E_{LL}}\right), \tag{12a}$$

$$\alpha_{TL} = V_{Tf}\left(\frac{\alpha_{fL}E_{fL}}{E_{TL}}\right) + \left(1 - V_{Tf}\right)\left(\frac{\alpha_{mL}E_{mL}}{E_{TL}}\right). \tag{12b}$$

The transverse CTE for each ply is:

$$\alpha_{LT} = V_{Lf}\left[\alpha_{fL} - v_f\left(\alpha_{LL} - \alpha_{fL}\right)\right] + \left(1 - V_{Lf}\right)\left[\alpha_{mL} - v_m(\alpha_{mL} - \alpha_{LL})\right], \tag{13a}$$

$$\alpha_{TT} = V_{Tf}\left[\alpha_{fT} - v_f\left(\alpha_{TL} - \alpha_{fT}\right)\right] + \left(1 - V_{Tf}\right)\left[\alpha_{mT} - v_m(\alpha_{mT} - \alpha_{TL})\right]. \tag{13b}$$

The calculated CTEs for each composite ply are given in Table 2. The resulting residual stresses in the transverse ply of each composite are estimated by balancing the forces and strains between the cross-plies:

$$t_L\sigma_{Lr} + t_T\sigma_{Tr} = 0, \tag{14}$$

$$\alpha_{LL}\Delta T + \epsilon_{Lr} = \alpha_{TT}\Delta T + \epsilon_{Tr}, \tag{15}$$

where ΔT=-75 °C is the change in temperature experienced by the sample after curing. Assuming each composite is still intact and a linear stress-strain relationship, the residual thermal stress in the transverse ply is:

$$\sigma_{Tr} = \frac{E_{TT}\Delta T(\alpha_{LL}-\alpha_{TT})}{1+{}^{E_{TT}t_T}/_{E_{LL}t_L}}. \quad (16)$$

The carbon and glass fiber composites are estimated to have residual, transverse ply stresses of 14.25 MPa and 11.80 MPa respectively. This level of stress is comparable to the axial stresses used to drive cracks in neat 2MEP4FS during the double cleavage drilled compression (DCDC) fracture test (Nielsen, 2012; Plaisted and Nemat-Nasser, 2007). At short crack lengths in the DCDC geometry, the tensile opening stress is approximately equal to the axial stress (Plaisted et al., 2006). Stress concentrations and interfaces created by the fibers are also expected to facilitate crack formation and propagation in the composite samples.

During mechanical characterization, tensile stresses due to bending may also generate cracks in the transverse plies. The maximum stress during single cantilever bending is expected near the grips and is estimated to be (TA Instruments, 2002):

$$\sigma_{TT\_max} = \frac{6d(t_L+t_T)F_cE_{TT}}{L^2\left[1+\frac{48}{5}(1+\nu)\left(\frac{t_L+t_T}{L}\right)^2\right]}. \quad (17)$$

Assuming intact lamina, DMA characterizations of the carbon and glass fiber composites are estimated to create maximum stresses of 1.15 MPa and 1.20 MPa respectively. Although these applied tensile stresses are in addition to the residual thermal stresses, they are significantly smaller in magnitude. Nairn and Hu (1992) notes that that progressive tensile loading of $[90,0]_s$ composites will lead to the generation of fewer and fewer new cracks until a saturation crack density is reached. This observation suggests the marginal increase in transverse ply tensile

stresses due to bending will create relatively few cracks compared with the initial residual thermal stresses due to CTE mismatches.

The effect of cracks on the mechanical properties of the composite samples was estimated using a shear lag model given by Lee and Daniel (1990). The model was developed for $[0,90]_s$ composites loaded in tension and is adapted here for application to $[90,0]_s$ composites subjected to bending. Others have successfully used shear lag models derived for tensile loading to estimate the mechanical properties of cross-ply composites in bending (Smith and Ogin, 1999, 2000). Here, the transverse ply cracks are assumed to be symmetric between the top and bottom layers (Figure 7). Longitudinal ply cracks are neglected as they will have minimal effect on the bending measurements due to their orientation.

The one-dimensional shear lag method for cross-ply composites assumes load is transferred from intact longitudinal plies to cracked transverse plies by shear stresses. The interfacial shear stress, τ_i, is considered proportional to the difference in average x-displacements between cross-plies ($\bar{u}_L$, $\bar{u}_T$):

$$\tau_i(x) = H[\bar{u}_T(x) - \bar{u}_L(x)], \tag{18}$$

where H is a shear lag parameter to be determined later. For a linear relationship between stress and strain and periodically spaced cracks, a normal stress distribution in each ply can be determined. The tensile stress between two cracks in a damaged transverse ply is:

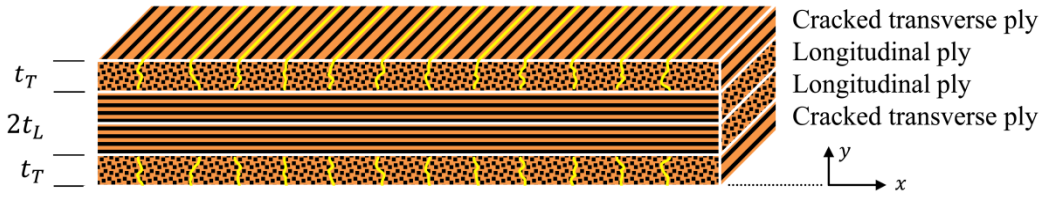

Fig. 7. The cracks in the transverse plies are assumed periodic and symmetric. Cracks in the longitudinal plies are not considered.

$$\sigma_{TT}^{*}(x) = \left(\frac{E_{TT}(t_L+t_T)}{E_{LL}t_L+E_{TT}t_T}\sigma_a + \sigma_{Tr}\right)\left(1 - \frac{cosh(\alpha S-\alpha x)}{cosh(\alpha S)}\right), \tag{19}$$

where σ_a is the applied stress, S is one half of the crack spacing, and:

$$\alpha^2 = H\left(\frac{1}{t_L E_{LL}} + \frac{1}{t_T E_{TT}}\right). \tag{20}$$

Neglecting the contribution of the transverse ply and assuming the average strain of the longitudinal plies is equal to the average strain of the entire composite, the average normal stress of the cracked transverse ply corresponds to an effective Young's modulus:

$$E_{TT}^{*} = \left(\frac{\alpha S - tanh(\alpha S)}{\alpha S + \frac{t_T E_{TT}}{t_L E_{LL}} tanh(\alpha S)}\right) E_{TT}. \tag{21}$$

Details of the calculations are given by Lee and Daniel (1990). The effective moduli of the damaged transverse plies are determined as a function of crack density in Figure 8.

To determine the shear lag parameter, H, for a composite subjected to bending, a parabolic variation in the shear stress distribution is assumed for each ply. For cubic variations of ply x-displacements through the thickness (y-direction):

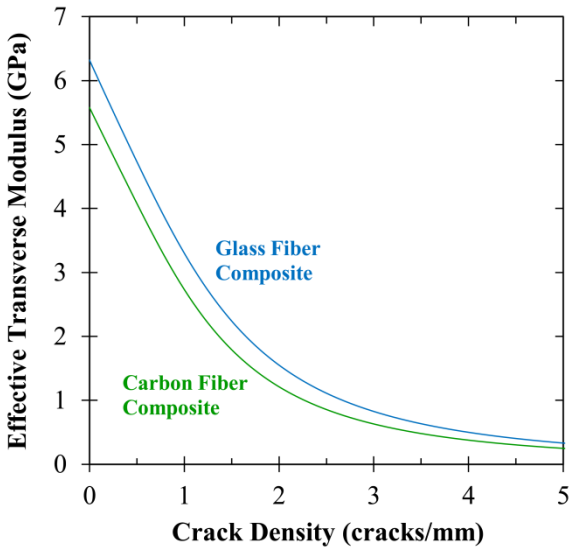

Fig. 8. Effective tensile Young's moduli of the cracked transverse plies.

$$u_L(x,y) = A_1(x)y^3 + A_2(x)y^2 + A_3(x)y + A_4(x), \tag{22a}$$

$$u_T(x,y) = B_1(x)y^3 + B_2(x)y^2 + B_3(x)y + B_4(x), \tag{22b}$$

the shear stresses can be approximated as:

$$\tau_L(x,y) = G_{LT}\frac{du_L(x,y)}{dy} = G_{LT}[3A_1(x)y^2 + 2A_2(x)y + A_3(x)], \tag{23a}$$

$$\tau_T(x,y) = G_{TT}\frac{du_T(x,y)}{dy} = G_{TT}[3B_1(x)y^2 + 2B_2(x)y + B_3(x)]. \tag{23b}$$

The boundary and continuity conditions are:

$$\tau_L(x, y = 0) = 0, \tag{24a}$$

$$u_L(x, y = t_L) = u_T(x, y = t_L), \tag{24b}$$

$$\tau_L(x, y = t_L) = \tau_T(x, y = t_L) = \tau_i(x), \tag{24c}$$

$$\frac{d\tau_L}{dy}(x, y = t_L) = 0, \tag{24d}$$

$$\frac{d\tau_T}{dy}(x, y = t_L) = 0, \tag{24e}$$

$$\tau_T(x, y = t_L + t_T) = 0. \tag{24f}$$

Averaging the displacements through the thickness and rearranging equation (18) gives the shear lag parameter:

$$H = \frac{12G_{LT}G_{TT}}{5(G_{LT}t_T + G_{TT}t_L)}. \tag{25}$$

The geometry and material properties are considered symmetric in this derivation of the shear lag parameter. Specifically, the boundary conditions suggest the cracks are open and must not close so the transverse laminate behaves similarly in compression as in tension. But microscopy observations indicate the cracks are mostly closed, and closed cracks are assumed in later beam bending analyses. A finite element simulation was used to verify the applicability of the determined shear lag parameter to the single cantilever bending of the carbon fiber composite sample with four closed cracks: one in each transverse ply at each DMA grip. Due to the

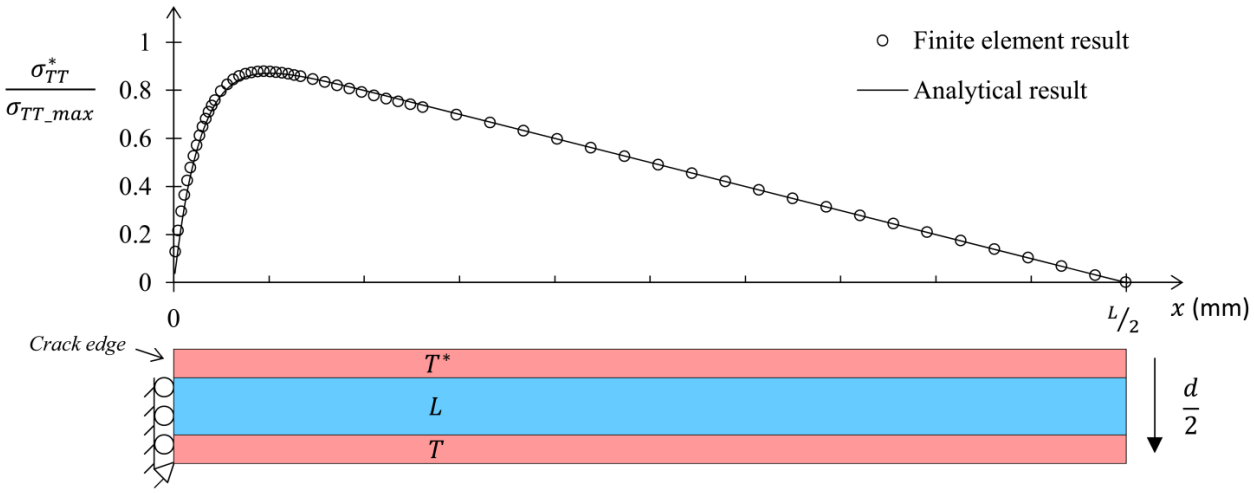

Fig. 9. One-half of the single cantilever DMA test on the carbon fiber composite was simulated using LS-DYNA. The average normal stress through the thickness of the cracked transverse ply ($\boldsymbol{T}^*$) was compared with the stress predicted by the shear lag model.

symmetry of the single cantilever experiment, one half of the sample was modeled (Figure 9) using 8112 plane strain shell elements and orthotropic material models with the previously determined effective properties (Table 2). At the fixed end, the longitudinal plies and transverse ply subjected to compression were fixed against x-displacement and in-plane rotation. The edge of the transverse ply experiencing tension was left free as a crack surface. At the opposite end of the sample, a periodic boundary condition was applied to all four layers and a uniform bending displacement $d/2$ was applied. The tensile transverse ply stress was averaged through the thickness of the ply at several locations and compared with the predicted stress distribution given by equation (19) (Figure 9). The correlation between the theoretical model and the finite element simulation is judged to be very good, indicating the shear lag parameter can be applied to analyses with closed cracks.

The effective properties of the damaged transverse plies are incorporated into the beam calculations. Assuming closed cracks, equation (8) is re-evaluated to find the neutral axis:

$$\bar{y} = \frac{4E_{LL}t_L(t_L+t_T)+t_T(4E^*_{TT}t_L+E_Tt_T+3E^*_{TT}t_T)}{4E_{LL}t_L+2t_T(E_{TT}+E^*_{TT})}, \quad (26)$$

and equation (10) is re-evaluated to find the overall flexural modulus:

$$E_{flex} = \frac{C_1+C_2+C_3}{16(t_L+t_T)^6}, \quad (27a)$$

where:

$$C_1 = 2E_{LL}t_L(4t_L^2 + 6t_L(t_T - \bar{y}) + 3(t_T - \bar{y})^2), \quad (27b)$$

$$C_2 = E_{TT}t_T(t_T^2 - 3t_T\bar{y} + 3\bar{y}^2), \quad (27c)$$

$$C_3 = E^*_{TT}t_T(12t_L^2 + 18t_Lt_T + 7t_T^2 - 12t_L\bar{y} - 9t_T\bar{y} + 3\bar{y}^2). \quad (27d)$$

The crack spacing parameter S is selected for each composite analysis such that the calculated flexural moduli matches the DMA measurements at room temperature. This fitting method gives crack densities of 3.21 cracks/mm and 2.23 cracks/mm for the carbon and glass fiber composites respectively. The calculations were also carried out as a function of temperature. Initially, the slow decline in the measured storage modulus is well predicted, but the experimental data eventually diverges, resulting in poor agreement at higher temperatures (Figure 12).

The estimated crack density for the glass fiber composite sample can be correlated with microscopy observations. Counting the number of transverse cracks in the through-thickness image (Figure 2) gives approximately 3.66 cracks/mm. Since longitudinal cracks are also apparent in the images, the observed transverse cracks may be from both transverse plies. Although the shear lag stress distribution assumes symmetric cracks, other researchers have noted that, in practice, transverse cracks in $[90,0]_s$ cross-ply composites tend to form in a staggered manner (Nairn and Hu, 1992). Assuming every crack is indeed staggered and visible, there are an estimated 1.83 cracks/mm in each 90° glass ply. The estimate of 2.23 cracks/mm is very reasonable given that not every crack may have been visible. The cracks are not ideally

periodic, and will tend to form at defects, which may lead to some being symmetric and therefore obscured from view. The observed number of cracks also does not include any additional cracks formed during DMA testing, but previous discussion has estimated the number of these cracks to be minimal. DMA measurements were observed to be reasonably consistent over all tests. Since the carbon fiber sample is not transparent, a similar correlation between analysis results and observations could not be made.

3.3. Composite with cracks that heal

The cracked composite approximation shows good agreement with the DMA measurements at low temperatures, while the ideal, intact composite approximation shows good agreement at high temperatures. This suggests the damage is being mitigated as the sample temperature is increased. One possibility is the cracks are slightly open at room temperature and progressively close without healing as the sample is heated and residual thermal strains are relieved. But crack closing would not increase the tensile modulus of the transverse plies, limiting the recovered bending stiffness of the composite. Additionally, the DMA measurements indicate the storage modulus doesn't immediately begin to diverge from the cracked assumption as would be expected if the cracks were closing. For these reasons and given the previously establishing healing capability of neat 2MEP4FS (Nielsen, 2012; Plaisted, 2007; Plaisted and Nemat-Nasser, 2007), the cracks are assumed to heal during the DMA temperature ramp experiments.

For healing to occur, the crack faces must directly abut, which will most truly occur near the crack tips. The crack tips in the 90° transverse plies are generally located near the longitudinal 0° plies where the cracks were arrested. It is expected that the cracks will first heal near this interface, and, as the temperature increases and thermal strain decreases, the cracks will continue to heal and the crack tips will retreat toward the free surface. As a simple model for this

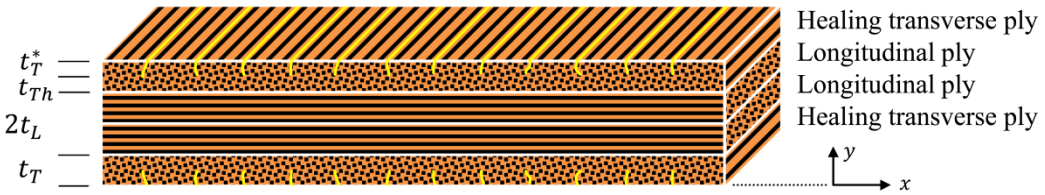

Fig. 10. The cracks in the transverse plies are assumed to heal. The transverse plies are subdivided into a healed layer and cracked layer with thicknesses related to the sample temperature.

assumed behavior, the transverse plies are separated into two layers: a healed layer with ideal properties and a cracked layer with the previously determined reduced modulus in tension (Figure 10). The thickness of each layer depends on the temperature, T, and the total ply thickness remains constant:

$$t_T = t_T^*(T) + t_{Th}(T). \tag{28}$$

Since the CTE of 2MEP4FS is approximately constant over the tested temperature range (Plaisted, 2007), the thickness of the healed layer, t_{Th}, is assumed to be a linear function of temperature. DSC measurements of 2MEP4FS with separated DA adducts show the adducts will begin to re-establish at ~48 °C (Nielsen, 2012) (Figure 11). The DSC measurements were made at the same average heating rate (3 °C/min) as was used for the DMA mechanical measurements. This temperature agrees with the observed onset of divergence between the DMA experimental results and the cracked composite calculations. During curing, the maximum temperature experienced by the samples was approximately 95 °C. This temperature is taken as the stress-free temperature for the composite, and the cracks are assumed to be fully healed. This is also the temperature Plaisted (Plaisted, 2007; Plaisted and Nemat-Nasser, 2007) used to finalize crack healing in neat 2MEP4FS and composite samples. The thickness of the healed transverse layer is then:

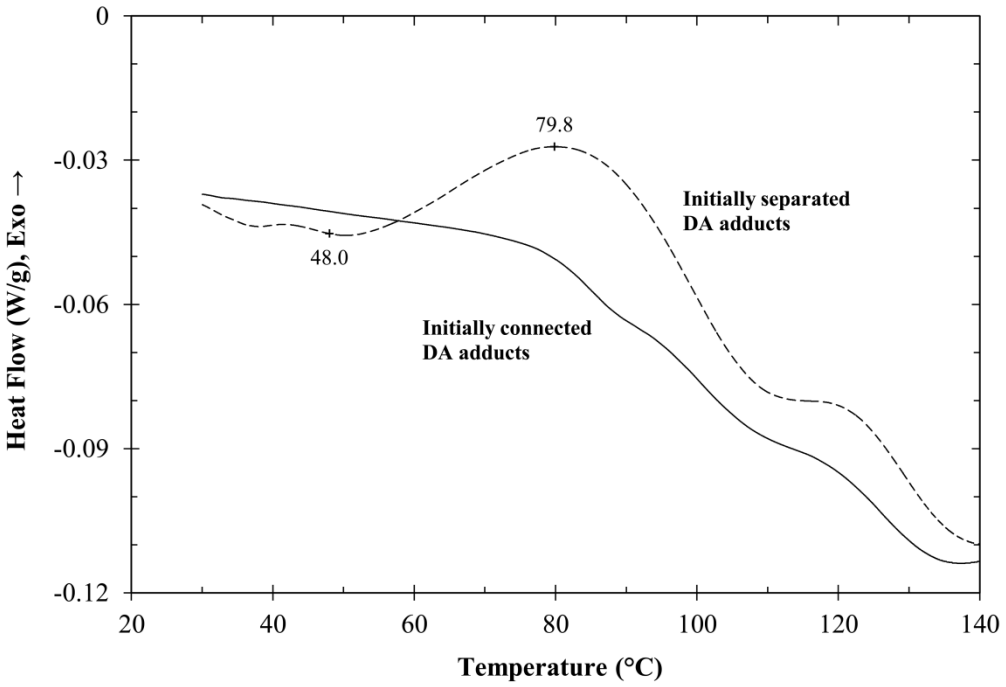

Fig. 11. A cured 2MEP4FS sample is DSC tested until a repeatable heat flow profile is obtained (solid line), and then quenched in liquid nitrogen. The sample is retested to observe the re-formation of DA bonds (dashed line). Data from Nielsen, 2012.

$$t_{Th} = \begin{cases} 0 & T < 48\ ℃ \\ \frac{T-48}{95-48} t_T & 48\ ℃ \le T \le 95\ ℃. \\ t_T & T > 95\ ℃ \end{cases} \tag{29}$$

The crack healing assumptions are used to calculate the composite beam properties as a function of temperature. For closed cracks, equation (8) gives the neutral axis as:

$$\bar{y}(T) = \frac{4E_{LL}t_L(t_L+t_T)+E_{TT}^{*}t_T^{*}(4t_L+4t_{Th}+3t_T^{*})+E_{TT}\left(4t_Lt_{Th}+(2t_{Th}+t_T^{*})^2\right)}{4E_{LL}t_L+2E_{TT}\left(2t_{Th}+t_T^{*}\right)+2E_{TT}^{*}t_T^{*}}. \tag{30}$$

and equation (10) gives the overall flexural modulus as:

$$E_{flex}(T) = \frac{D_1+D_2+D_3}{16(t_L+t_T)^6}. \tag{31a}$$

where,

$$D_1 = E_{LL}((2t_L + t_T - \bar{y})^3 - (t_T - \bar{y})^3), \tag{31b}$$

$$D_2 = E_{TT}((2t_L + 2t_{Th} + t_T^* - \bar{y})^3 - (2t_L + t_T - \bar{y})^3 + (t_T - \bar{y})^3 + \bar{y}^3), \quad (31c)$$

$$D_3 = E_{TT}^*((2t_L + 2t_T - \bar{y})^3 - (2t_L + 2t_{Th} + t_T^* - \bar{y})^3). \quad (31d)$$

The temperature dependent flexural modulus, equation (31), is compared with the DMA measurements in Figure 12, and the correlation is deemed excellent over the entire temperature range. Small deviations in the glass fiber composite results could be attributed to inconsistent crack paths. The cracks observed by microscopy were generally more torturous in the glass fiber sample than the carbon fiber sample, with more branching and more variation in the x-direction. This may be due to differences in filament size (10 μm glass diameter (AGY, 2006), 7 μm carbon diameter (Toray Carbon Fibers America Inc, 2012)) and interfacial shear strength.

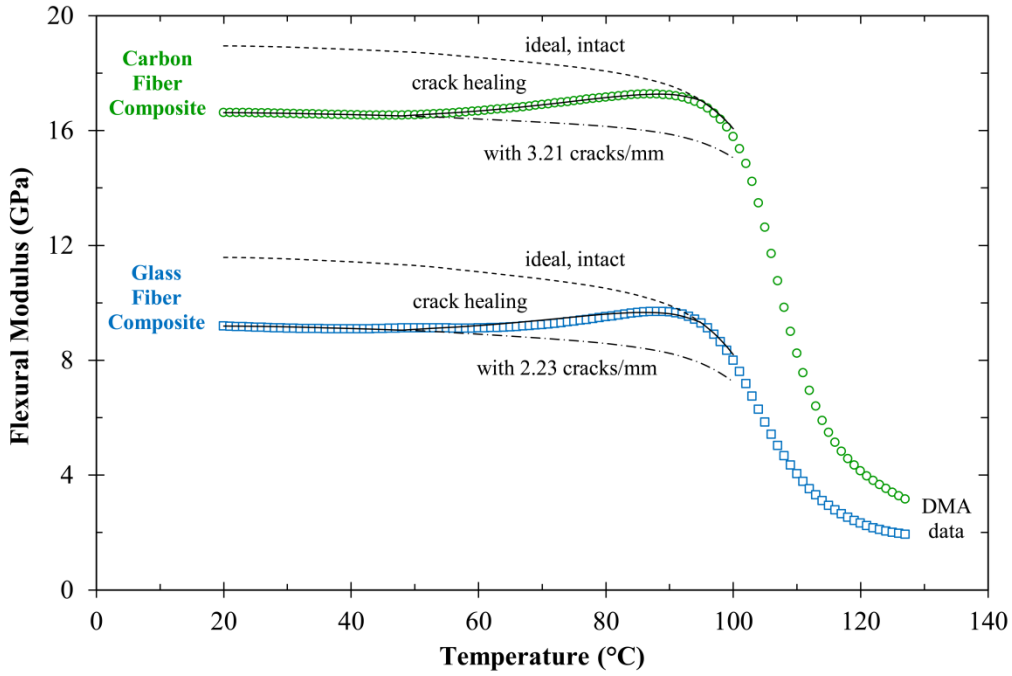

Fig. 12. The various composite analyses compared with the DMA experimental measurements.

4. Discussion and conclusions

Carbon and glass fiber cross-ply composites were characterized, and analytical approximations were used to describe the observed behavior. The experimental and analytical results indicate crack healing occurs as the sample temperature is increased. Healing was not directly observed however, due to the elevated temperatures and closed DMA instrument. Examining the samples after DMA characterization, the cracks that were observed before testing were still observed after testing. Since the sample was cooled back to room temperature, the residual thermal stresses returned and re-formed the cracks. The crack locations are controlled by the stress distribution and local defects, which would still be present after testing. Identical crack paths suggest incomplete healing at the fiber-matrix interface. Previous studies that showed ideal healing were for the neat 2MEP4FS polymer (Plaisted and Nemat-Nasser, 2007).

Since the cracks re-formed in the same locations, it is difficult to claim the samples were completely healed, even at elevated temperatures and despite the analytical results. Due to the essentially zero thickness of the cracks relative to the length of the sample, even poor crack healing that barely holds the crack faces together would have a dramatic impact on DMA bending measurements. Similar DMA experiments on other composite samples with functionalized glass fibers have demonstrated that fiber surface treatments have a minimal impact on the measured properties despite large changes in the interfacial bonding strength (Jia et al., 2012). At the small strains used by the DMA, the quality of the interface isn't being evaluated. Beam bending measurements and analyses are also very sensitive to sample thickness. The ply thicknesses were estimated based on observations of the sample edges. Variations in these thicknesses through the unseen regions of the sample would strongly affect the measured results, as well as the estimated number of cracks needed to match the analytical

and experimental results at room temperature. The number of cracks in the shear lag analysis is controlled by the shear moduli of the plies, which were estimated here by particularly crude methods. Given the good agreement between the number of estimated and observed cracks in the glass fiber composite sample, the ply thicknesses and shear moduli used in the analyses appear reasonable.

Each sample was only tested as a function of temperature once. Retesting the samples would give incomparable results as the gripped regions had permanently deformed during the high temperature portion of the tests. In order to observe crack healing in the composite samples, additional thermal treatments could be used to increase the damage present in the samples before testing. By initially cooling the samples below room temperature, new cracks would be generated that should remain healed during microscopy observations after DMA characterization. Following this approach, Plaisted (2007) successfully observed composite crack healing.

The composite samples were only characterized at only one level of damage. Progressively imparting additional cracks would allow the shear lag model to be better compared with experimental measurements. A fracture criterion could be developed and an energy release rate estimated. More complex, variational methods for stress analysis in cracked cross-ply composites have been developed (Hashin, 1996; Nairn, 1989) and deemed more accurate for developing fracture criteria (Nairn et al., 1993). An energy release rate would be useful for evaluating the fiber-matrix interface and interfacial healing. The experimental methods given in the literature for developing a fracture criterion require relatively large samples, which would be difficult to produce with material quantities limited by current processing methods. Adaptation of the methods for use with the healable materials is left for future efforts.

Acknowledgements

The authors thank Haim Weizman and Dmitriy Uchenik for synthesizing the monomers used in this study. Alireza V. Amirkhizi and Wiroj Nantasetphong are also gratefully acknowledged for the helpful conversations. This work was funded by Air Force Office of Scientific Research grant FA9550-08-1-0314 to UC San Diego.

References

AGY. High strength glass fibers: technical paper. Aiken: AGY, 2006.

Chen X, Dam MA, Ono K, et al. A thermally re-mendable cross-linked polymeric material. *Science* 2002; 295: 1698-1702.

Chen X, Wudl F, Mal AK, et al. New thermally remendable highly cross-linked polymeric materials. *Macromolecules* 2003; 36: 1802-1807.

Hashin Z. Analysis of stiffness reduction of cracked cross-ply laminates. *Eng Fract Mech* 1986; 25: 771-778.

Hashin Z. Finite thermoelastic fracture criterion with application to laminate cracking analysis. *J Mech Phys Solids* 1996; 44: 1129-1145.

Highsmith AL and Reifsnider KL. Stiffness-reduction mechanisms in composite laminates. In: Reifsnider KL (ed) *Damage in composite materials: basic mechanics, accumulation, tolerance, and characterization*. ASTM STP 775; 1982. p. 103-17.

Jia Z, Holzworth K and Nemat-Nasser S. Milled glass reinforced polyurea composites: the effect of surface treatment. *Proceedings of the Society for Experimental Mechanics Annual Conference*. Costa Mesa, CA; 2012.

Kaw AK. *Mechanics of composite materials*. 2nd ed. Boca Raton: CRC Press, 2006.

Laws N and Dvorak GJ. Progressive transverse cracking in composite laminates. *J Compos Mater* 1988; 22: 900-916.

Lee JW and Daniel IM. Progressive transverse cracking of crossply composite laminates. *J Compos Mater* 1990; 24: 1225-1242.

Nairn JA. The strain energy release rate of composite microcracking: a variational approach. *J Compos Mater* 1989; 23: 1106-1129.

Nairn JA and S Hu. The formation and effect of outer-ply microcracks in cross-ply laminates: a variational approach. *Eng Fract Mech* 1992; 41: 203-221.

Nairn JA, Shoufeng H and Bark JS. A critical evaluation of theories for predicting microcracking in composite laminates. *J Mater Sci* 1993; 28: 5099-5111.

Nemat-Nasser S and Hori M. *Micromechanics: overall properties of heterogeneous materials*. 2nd ed. Amsterdam: Elsevier, 1999.

Nielsen C. *On healable polymers and fiber-reinforced composites*. PhD Thesis, University of California at San Diego, USA, 2012.

Nielsen C, Weizman H and Nemat-Nasser S. Thermally reversible cross-links in a healable polymer: estimating the quantity, rate of formation, and effect on viscosity. *Polymer* 2014; 55: 632-641.

Pang JWC and Bond IP. A hollow fibre reinforced polymer composite encompassing self-healing and enhanced damage visibility. *Compos Sci Technol* 2005; 65: 1791-1799.

Park JS, Kim HS and Hahn HT. Healing behavior of a matrix crack on a carbon fiber/mendomer composite. *Compos Sci Technol* 2009; 69: 1082-1087.

Plaisted TA, Amirkhizi AV and Nemat-Nasser S. Compression-induced axial crack propagation in DCDC polymer samples: experiments and modeling. *Int J Fract* 2006; 141: 447-457.

Plaisted TA. *Multifunctional composites: healing, heating and electromagnetic integration*. PhD Thesis, University of California at San Diego, USA, 2007.

Plaisted TA and Nemat-Nasser S. Quantitative evaluation of fracture, healing and re-healing of a reversibly cross-linked polymer. *Acta Mater* 2007; 55: 5684-5696.

Sjögren BA and Berglund LA. The effects of matrix and interface on damage in GRP cross-ply laminates. *Compos Sci Technol* 2000; 60: 9-21.

Smith PA and Ogin SL. On transverse matrix cracking in cross-ply laminates loaded in simple bending. *Compos Part A-Appl S* 1999; 30: 1003-1008.

Smith PA and Ogin SL. Characterization and modelling of matrix cracking in a (0/90)2s GRFP laminate loaded in flexure. *P Roy Soc A-Math Phy* 2000; 456: 2755-2770.

TA Instruments. DSC 2920: differential scanning calorimeter operator's manual. New Castle: TA Instruments-Waters LLC, 1998.

TA Instruments. DMA 2980: dynamic mechanical analyzer operator's manual. New Castle: TA Instruments-Waters LLC, 2002.

Toohey KS, Sottos NR, Lewis JA, et al. Self-healing materials with microvascular networks. *Nat Mater* 2007; 6: 581-585.

Toray Carbon Fibers America Inc. Torayca T300 data sheet: technical data sheet CFA-001. Santa Ana: Toray Carbon Fibers America Inc, 2012.

White SR, Sottos NR, Guebelle PH, et al. Autonomic healing of polymer composites. *Nature* 2001; 409: 794-797.

Weizman H, Nielsen C, Weizman OS, et al. Synthesis of a self-healing polymer based on reversible Diels-Alder reaction: an advanced undergraduate laboratory at the interface of organic chemistry and materials science. *J Chem Educ* 2011; 88: 1137-1140.

Wool RP and O'Conner KM. A theory of crack healing in polymers. *J Appl Phys* 1981; 52: 5953-5963.

Vitae

Christian Nielsen

Christian Nielsen received his B.S. degree from Case Western Reserve University in 2006 and M.S. and Ph.D. degrees from the University of California at San Diego in 2008 and 2012 respectively. He is currently a postdoctoral researcher at UCSD's Center of Excellence for Advanced Materials. His research is focused on developing and characterizing multifunctional materials.

Sia Nemat-Nasser

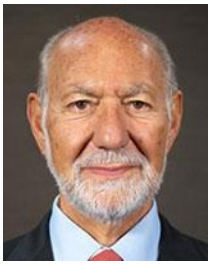

Sia Nemat-Nasser is Distinguished Professor of Mechanics and Materials at the University of California at San Diego and director of UCSD's Center of Excellence for Advanced Materials. He received his B.S. degree from Sacramento State University in 1960 and M.S. and Ph.D. degrees from the University of California at Berkeley in 1961 and 1964 respectively. He is a member of the National Academy of Engineering and has received numerous awards, including the William Prager Medal, Stephen P. Timoshenko Medal, Theodore von Karman Medal, and ASME Medal. His research integrates experiment, theory, and computation in studying the mechanics of solids.